THE ASTROPHYSICAL JOURNAL, 542:597–607, 2000 October 20

ON COOLING FLOWS AND THE SUNYAEV-ZELDOVICH EFFECT

SUBHABRATA MAJUMDAR[1,2] AND BIMAN B. NATH[3]
Received 2000 January 27; accepted 2000 May 24

ABSTRACT

We study the effect of cooling flows in galaxy clusters on the Sunyaev-Zeldovich (SZ) distortion and the possible cosmological implications. The SZ effect, along with X-ray observations of clusters, is used to determine the Hubble constant, H_0. Blank-sky surveys of SZ effect are being planned to constrain the geometry of the universe through cluster counts. It is also known that a significant fraction of clusters have cooling flows in them, which change the pressure profile of intracluster gas. Since the SZ decrement depends essentially on the pressure profile, it is important to study possible changes in the determination of cosmological parameters in the presence of a cooling flow. We build several representative models of cooling flows and compare the results with the corresponding case of gas in hydrostatic equilibrium. We find that cooling flows can lead to an overestimation of the Hubble constant. Specifically, we find that for realistic models of cooling flow with mass deposition (varying $\dot{m}$ with radius), there is of the order of $\sim 10\%$ deviation in the estimated value of the Hubble constant (from that for gas without a cooling flow) even after excluding $\sim 80\%$ of the cooling-flow region from the analysis. We also discuss the implications of using cluster counts from SZ observations to constrain other cosmological parameters in the presence of clusters with cooling flows.

Subject headings: cooling flows — cosmic microwave background — distance scale — galaxies: clusters: general — large-scale structure of universe

1. INTRODUCTION

Galaxy clusters have been extensively observed in optical, X-ray, and radio bands. In the radio band, a cluster can be observed on the Rayleigh-Jeans (RJ) side of the cosmic microwave background spectrum as a dip in the brightness temperature, due to the Sunyaev-Zeldovich (SZ) effect (Sunyaev & Zeldovich 1972; for a comprehensive review, see Birkinshaw 1999). The SZ distortion appears as a decrement for wavelengths ≥ 1.44 mm (frequencies ≤ 218 GHz), and as an increment for wavelengths ≤ 1.44 mm. The SZ effect has the advantage that the SZ intensity, unlike the X-ray, does not suffer from the $(1+z)^{-4}$ cosmological dimming. As discussed by numerous authors (Birkinshaw & Hughes 1994; Silverberg et al. 1997), one can combine the X-ray and radio observations for clusters to determine cosmological parameters. This has been done in the recent years to determine the Hubble constant, H_0 (Birkinshaw 1999). The SZ signal, however, is weak and difficult to detect. Recent high signal-to-noise ratio detections have been made over a wide range of wavelengths using single-dish observations at radio wavelengths (Herbig et al. 1995; Hughes & Birkinshaw 1998), millimeter wavelengths (Holzapfel et al. 1997; Pointecouteau et al. 1999), and submillimeter wavelengths (Komatsu et al. 1999). Interferometric observations have also been carried out to image the SZ effect (Jones et al. 1993; Saunders et al. 1999; Reese et al. 2000; Grego et al. 2000). In addition to estimating H_0 by combining SZ and X-ray data, the SZ effect alone can also be used to determine the cosmological mass density of the universe, Ω_0 (Bartlett & Silk 1994; Oukbir & Blanchard 1992, 1997; Blanchard & Bartlett 1998). However, these procedures generally assume that the cluster gas is spherical, unclumped, and isothermal. Almost all clusters, however, show departures from these assumptions, some to a large extent.

Departures from these simple assumptions can lead to systematic errors in the determination of the different cosmological parameters (Inagaki, Suginohara, & Suto 1995); in particular, it has been shown that nonisothermality of the cluster can lead to a substantial error in the values of the cosmological parameters. Temperature structure in a cluster can be the result of the shape of the gravitational potential (Navarro, Frenk, & White 1997; Makino, Sasaki, & Suto 1998), or it can arise from the fact that the initial falling gas in the cluster potential is less shock heated than the later falling gas (Evrard 1990). In fact, hydrodynamical simulations of isolated clusters also show a definite temperature structure and can introduce error in the value of H_0 compared to the traditional isothermal β-models (Yoshikawa, Itoh, & Suto 1998). Roettiger, Stone, & Mushotzky (1997) have shown that cluster mergers can result in deviations from both sphericity and isothermality. Observationally, the main handicap arises from the fact that the thermal structures of clusters are difficult to measure, and the temperatures generally taken in analyses are the X-ray emission weighted temperature, usually measured over a few core radii. Thus, in general an isothermal description of the cluster is taken (or sometimes a phenomenological temperature model based on the Coma cluster; see, e.g., eq. [73] of Birkinshaw 1999).

In this paper, we study another important phenomenon that can substantially change the temperature structure, viz., a cooling flow. The existence of cooling flows in clusters of galaxies (for an introduction, see Fabian, Nulsen, & Canizares 1984) is a well-established fact by now, and it is apparent that around 60%–90% of clusters exhibit cooling

[1] Joint Astronomy Programme, Physics Department, Indian Institute of Science, Bangalore 560012, India.
[2] Indian Institute of Astrophysics, Koramangala, Bangalore 560034, India.
[3] Raman Research Institute, Bangalore 560080, India.

flows in their core, with $\approx 40\%$ of them having cooling flows of more than 100 $M_\odot$ yr^{-1} (Markevitch et al. 1998; Peres et al. 1998; Allen et al. 1999). In the largest systems, the mass deposition rate can be as high as 1000 $M_\odot$ yr^{-1} (Allen 2000). The idealized picture of a cooling flow is as follows. Initially, when the cluster forms, the infalling gas is heated from gravitational collapse. With time this gas cools slowly, and a quasi-hydrostatic state emerges. However, in the central region, where energy is lost due to radiation faster than elsewhere, an inward "cooling flow" initially arises as a result of the pressure gradient (Fabian 1994). This can modify the SZ decrement and act as a systematic source of error in the determination of the cosmological parameters.

Schlickeiser (1991) has shown that free-free emission from cold gas in the cooling flow can actually lead to an apparent decrease of the SZ effect at the center. Since the central cooling flow region is generally very small, the isothermal β-model of cluster gas can still be used for the majority of the cluster region even for a cooling flow cluster, with the extra precaution of excluding the central X-ray spike from the X-ray fit, and a corresponding change made in the fitting of the SZ decrement. However, this is only possible for nearby clusters with well-resolved cluster cores.

Naively, the change in the central SZ decrement $y(0)$ can be seen as follows. For a non–cooling-flow cluster, the central decrement is given by the line-of-sight integral of the electron pressure through the cluster center along the full extent of the cluster. If the cluster has a maximum radius $r_{\rm cl}$, then the central SZ decrement at RJ wavelengths can be written as $y(0) = -4[\sigma_{\rm T}/(m_e c^2)]\int_0^{r_{\rm cl}} p_e\, dl$. For a cluster with a cooling flow, let us suppose that the electron pressure, p_e, falls drastically below a certain radius r_s, which is typically well inside the core of the cluster. The resulting central decrement is then $y(0) \approx -4[\sigma_{\rm T}/(m_e c^2)]\int_{r_s}^{r_{\rm cl}} p_e\, dl$. Depending on the distance of r_s from the cluster center [$r_s \approx (0.1\text{–}0.3) r_{\rm core}$], there will be a change in the value of $y(0)$ by $\approx 5\%$–25%. However, this simplistic view may not be true. This estimate assumes that the pressure profile remains a β profile outside the radius r_s. The pressure profile, however, need not follow the β profile once the cooling flow starts, and it can deviate from it substantially even for radii much larger than r_s. As a matter of fact, there can actually be an increase in the pressure for a large region inside the cooling flow, before a sudden drop inside r_s. Since the usual procedure for estimating the Hubble constant depends on fitting β profiles to the SZ and X-ray profiles, to estimate $r_{\rm core}$, this change in the pressure profile due to a cooling flow can distort the estimation of $r_{\rm core}$, and hence the value of H_0, in a nontrivial way. We study this effect in detail in later sections.

In this paper, we have investigated the problem of cooling-flow–induced changes in the temperature and density profile, its effect on the SZ effect, and its subsequent effect on the determination of cosmological parameters. In § 2 we briefly review the physics of the SZ effect; § 3 is devoted to the physics of cooling flows and discussing the cooling-flow solutions; in § 4 we look at the effect of cooling-flow solutions on the SZ effect in the determination of both H_0 and Ω_0; we conclude in § 5 with a brief comment on how this work differs from other works and the relevance of this paper. For the SZ effect, our notation and approach mainly follows that described in Barbosa et al. (1996b).

2. DETERMINING THE HUBBLE CONSTANT WITH THE SUNYAEV-ZELDOVICH EFFECT

2.1. *The Sunyaev-Zeldovich Effect*

The integral of the electron pressure along any line of sight through the cluster determines the magnitude of the distortion of the apparent brightness temperature of the cosmic microwave background (CMB) due to the SZ effect. This is quantified in terms of the Compton y-parameter,

$$y = \int dl\, \frac{k_{\rm B} T_e}{m_e c^2}\, n_e \sigma_{\rm T}\,, \tag{1}$$

where $k_{\rm B}$ is the Boltzman constant, T_e is the gas temperature, m_e is the electron rest mass, n_e is the electron number density, c is the velocity of light, and $\sigma_{\rm T}$ is the Thomson scattering cross section. This occurs through the inverse Compton scattering, by the hot intracluster gas, of the CMB photons propagating through the cluster medium, and the energy transfer in this interaction between hot electrons and CMB photons, resulting in a distortion to the CMB spectrum. The SZ surface brightness at a position θ of the cluster with respect to the mean CMB intensity is given by

$$\delta i_\nu(\theta) = y(\theta) j_\nu(x)\,, \tag{2}$$

where x is a dimensionless frequency parameter,

$$x = \frac{h\nu}{kT_0}\,, \tag{3}$$

where h is the Planck constant, ν is the observing frequency, and T_0 is the CMB temperature at the present epoch: $T_0 \sim 2.73$ K. The function $j_\nu(x)$ describes the spectral shape of the effect,

$$j_\nu(x) = \frac{2(kT_0)^3}{(hc)^2}\, \frac{x^4 e^x}{(e^x - 1)^2} \left[\frac{x}{\tanh\,(x/2)} - 4 \right]. \tag{4}$$

Since the total photon number is conserved in the inverse Compton scattering process (upscattering of the photons), the spectral dependence gets a unique shape through a decrement in the brightness temperature at lower frequencies, while an increase is observed at higher frequencies.

The Sunyaev-Zeldovich effect provides a unique observing approach to traditional methods, which use X-ray temperature and X-ray luminosity. The X-ray studies have a major disadvantage because of "cosmological dimming": the surface brightness of distant X-ray sources falls off as $(1 + z)^{-4}$, and for this reason, obtaining samples of clusters at cosmological distances is challenging. The SZ effect has the distinct advantage of being independent of the distance to the cluster. The SZ flux density from a cluster will diminish with distance to the cluster as the square of the angular-size distance, in contrast to X-ray flux densities from clusters, which diminish as the square of the luminosity distance to the cluster. If the observations resolve clusters, particularly at lower redshifts, the observed sky SZ temperature distribution will be sensitive to the thermal electron temperature structure within the clusters; once again, this can be contrasted with X-ray emission images of cluster gas distributions, which are mainly sensitive to the gas density distribution.

2.2. *Determination of the Hubble Constant*

The method for determining the Hubble constant using the Sunyaev-Zeldovich effect uses two observable quan-

tities: (1) $\Delta T/T$ of the CMB due to the SZ effect, and (2) the X-ray surface brightness, S_X, of the cluster. These can be written as

$$\frac{\Delta T_{SZ}}{T}(r) = -2\int_{l_{min}}^{l_{max}} \frac{k_B T_e}{m_e c^2}\sigma_T n_e\, dl\,, \tag{5}$$

$$S_X(r) = \frac{1}{4\pi(1+z)^4}\int_{l_{min}}^{l_{max}} \frac{dL_X}{dV}dl\,, \tag{6}$$

where r is the distance to the line of sight from the cluster center, l_{max} and l_{min} give the extension of the cluster along the line of sight, dL_X/dV is the X-ray emissivity, and dl is the line element along the line of sight. The X-ray emissivity in the frequency band $\nu = \nu_1 - \nu_2$ can be written as

$$\frac{dL_X}{dV} = n_e^2\,\alpha(T_e;\,\nu_1,\,\nu_2,\,z)\,, \tag{7}$$

where

$$\alpha(T_e;\,\nu_1,\,\nu_2,\,z) = \frac{2}{1+X}\left(\frac{2\pi}{3m_e c^2}\right)^{1/2} \times \frac{16e^6}{3\hbar m_e c^2}\,A(T_e;\,\nu_1,\,\nu_2,\,z)\,, \tag{8}$$

where

$$A(T_e;\,\nu_1,\,\nu_2,\,z) = \int_{u_1(1+z)}^{u_2(1+z)} (k_B T_e)^{1/2} e^{-u} \times [X g_{ff}(T_e,\,u,1) + (1-X) g_{ff}(T_e,\,u,2)]\,du\,. \tag{9}$$

In the above equations we have assumed a primordial abundance of hydrogen and helium, and have set $X = 0.76$; e is the electron charge, $\hbar = h/(2\pi)$, $u \equiv 2\pi\hbar\nu/k_B t_e$, and $g_{ff}(T_e, u, Z)$ is the velocity-averaged Gaunt factor for the ion of charge Ze (Kellog, Baldwin, & Koch 1975). Traditionally, to model the cluster gas distribution one takes the following density and temperature profiles (Cavaliere & Fusco-Femiano 1978):

$$n_e(r) = n_{e0}\left[1 + \left(\frac{r}{r_{core}}\right)^2\right]^{-3\beta/2}\,, \tag{10}$$

$$T_e(r) = T_{iso} = \text{const}\,, \tag{11}$$

where n_{e0} is the central electron density and r_{core} is the core radius of the cluster. The above expressions are used as an empirical fitting model, and the parameter β is regarded as the fitting parameter. The equation holds for $0 < r < R_{cl}$, where R_{cl} is the maximum "effective" extension of the cluster. Conventionally, $R_{cl} = \infty$, and then from equations (5), (6), (10), and (11) we get

$$\frac{\Delta T_{SZ}}{T}(\theta) = -\frac{2\sqrt{\pi}\sigma_T k_B T_{iso}}{m_e c^2} n_{e0} r_{core} \times \frac{\Gamma(3\beta/2 - 1/2)}{\Gamma(3\beta/2)}\left[1 + \left(\frac{d_A\theta}{r_{core}}\right)^2\right]^{1/2-3\beta/2}\,, \tag{12}$$

$$S_X(\theta) = \frac{\sqrt{\pi}}{4\pi(1+z)^4}\alpha n_{e0}^2 r_{core} \times \frac{\Gamma(3\beta - 1/2)}{\Gamma(3\beta)}\left[1 + \left(\frac{d_A\theta}{r_{core}}\right)^2\right]^{1/2-3\beta}\,, \tag{13}$$

where $\Gamma(x)$ is the gamma function. Since both the central CMB decrement and the X-ray surface brightness are observed, one can then combine equations (12) and (13) to estimate the core radius as

$$r_{c,est} = \frac{[\Delta T(\theta)/T]^2_{obs}}{S_X(\theta)_{obs}} \frac{\Gamma(3\beta - 1/2)\Gamma(3\beta/2)^2}{\Gamma(3\beta/2 - 1/2)^2\Gamma(3\beta)} \times \frac{m_e^2 c^4 \alpha}{16\pi^{3/2}(1+z)^4\sigma_T k_B T_{e,fit}^2} \times \left[1 + \left(\frac{\theta}{\theta_{X,core}}\right)^2\right]^{-1/2}\,. \tag{14}$$

In the above equation, $\theta_{X,core}$ is the angular core radius observed in the X-ray, and $T_{e,fit}$ is the X-ray flux–averaged temperature (obtained from fitting the observed X-ray spectrum to the theoretical spectrum expected from isothermal case). This X-ray emission–weighted temperature is given by

$$T_{iso} \equiv \frac{\int_0^{r_{vir}} T_e(r)\alpha n_e^2 r^2\,dr}{\int_0^{r_{vir}} \alpha n_e^2 r^2\,dr}\,. \tag{15}$$

The point to be noted is that r_{vir} is the virial radius of the cluster, and its choice depends on the observer. If the temperature has a spatial structure, then the T_{iso} inferred from such a procedure may give different values depending on how much of the cluster is taken in making the above average. It has been shown (Yoshikawa et al. 1998) that this can lead to a substantial change in the SZ effect inferred, and thus to the value of H_0.

The angular-diameter distance, d_A, can be approximated for nearby ($z \ll 1$) clusters as

$$d_A = \frac{cz}{H_0}\left[1 + \frac{2\Lambda - \Omega_0 - 6}{4}z + O(z^2)\right]. \tag{16}$$

Thus, we finally have an estimate of $d_A(z)$ as $r_{c,est}/\theta_{X,core}$. If from other observations we know the cosmological parameters Ω_0 and Λ, then we can estimate the Hubble constant.

As can be seen from the above equations, the value of H_0 depends crucially on the many assumptions of the isothermality and β-model density distribution of the cluster. Cooling flows change both of these, and so can significantly affect the value of the Hubble constant.

3. COOLING FLOWS IN CLUSTERS

3.1. *Preliminaries*

From X-ray spectra of clusters, it is known that the continuum emission is thermal Bremsstrahlung in nature and originates from diffuse intracluster gas with densities of 10^{-2}–10^{-4} cm^{-3} and temperatures around 10^7–10^8 K. The gas is usually believed to be in hydrostatic equilibrium. If, however, the density in the inner region is large enough that the cooling time is less than the age of the cluster, then there is a "cooling flow" (Fabian et al. 1984 and references therein). Of course, there would be a flow only when the dynamical time is also shorter than the cooling timescale ($t_{age} > t_{cool} > t_{dyn}$).

The basic equations of cooling flow are:

$$\frac{du}{dr} = -\frac{u}{\rho_b}\frac{d\rho_b}{dr} - \frac{2u}{r} - \frac{\dot{\rho}_b}{\rho_b}\,,$$

$$u\frac{du}{dr}+\frac{1}{\rho_b}\frac{d(\rho_b\theta)}{dr}=-\frac{GM_t(r)}{r^2},$$
$$u\frac{d}{dr}\left(\frac{3\theta}{2}\right)-\frac{\theta u}{\rho_b}\frac{d\rho_b}{dr}=\frac{\rho\Lambda(\theta)}{(\mu m_p)^2}, \quad (17)$$

where $\theta = 2k_B T/\mu m_p$, μ is the mean molecular weight, and m_p is the proton mass. For steady flows with constant mass flux, $\dot{\rho} = 0$. This implies $u = \dot{m}/4\pi\rho r^2$ for steady flows. (Note that in cooling flows both u and $\dot{m}$ are negative. The subscripts b denotes baryons, and t denotes total, i.e., baryons + dark matter. However, we assume that the baryonic contribution to the total mass is negligible with respect to the dark matter contribution.)

The term $M(r)$ describes the distribution of the total mass and depends on the details of dark matter density profiles (see below), and $\Lambda(\theta)$ is the cooling function, defined so that $n_e n_p \Lambda(\theta)$ is the rate of cooling per unit volume. We use an analytical fit to the optically thin cooling function as given by Sarazin & White (1987),

$$\frac{\Lambda(\theta)}{10^{-22}\ \mathrm{ergs\ cm^3\ s^{-1}}} = 4.7\times\exp\left[-\left(\frac{T}{3.5\times10^5\ \mathrm{K}}\right)^{4.5}\right]$$
$$+0.313\times T^{0.08}\exp\left[-\left(\frac{T}{3.0\times10^6\ \mathrm{K}}\right)^{4.4}\right]$$
$$+6.42\times T^{-0.2}\exp\left[-\left(\frac{T}{2.1\times10^7\ \mathrm{K}}\right)^{4.0}\right]$$
$$+0.000439\times T^{0.35}. \quad (18)$$

This fit is accurate to within 4% for a plasma with solar metallicity within $10^5 \le T \le 10^8$ K. For $10^8 \le T < 10^9$ K, it underestimates cooling by a factor of order unity (compared to the exact cooling function, as in, e.g., Schmutzler & Tscharnuter 1993), and therefore is a conservative fit as far as the effect of cooling is concerned.

For nonsteady flows, we adopt the formalism of White & Sarazin (1987), who characterize the mass deposition rate, $\dot{\rho}$, by a "gas-loss efficiency" parameter, q. One writes $\dot{\rho} = q(\rho/t_{\mathrm{cool}})$, where t_{cool} is the local isobaric cooling rate ($t_{\mathrm{cool}} = 5k_B T\mu m_p/\rho\Lambda$). It has been found that $q \sim 3$ models can reproduce the observed variation of mass flux ($\dot{m} \propto r$; Sarazin & Graney 1991). Fabian (1994) has noted that these models of White & Sarazin (1987) yield good approximations to the emission-weighted mean temperature and density profiles for cooling-flow clusters. We also note that Rizza et al. (2000) have used the steady-flow models of White & Sarazin (1987) to simulate cooling flows.

We first discuss cooling flows with $\dot{m} = \mathrm{const}$. With $q = 0$, one can eliminate the density from equation (17) to get two differential equations:

$$\frac{du}{dr}=\frac{u}{[r^2(5\theta-3u^2)]}\left[3GM-10r\theta+\frac{\dot{m}}{2\pi}\frac{\Lambda(\theta)}{uM^2}\right],$$
$$\frac{d\theta}{dr}=\frac{2}{[r^2(5\theta-3u^2)]}$$
$$\times\left[\theta(2u^2r-GM)-(u^2-\theta)\frac{\dot{m}}{4\pi}\frac{\Lambda(\theta)}{uM^2}\right]. \quad (19)$$

These equations have singularities at the sonic radius r_s, where $5\theta_s = 3u_s$. A necessary condition of singularity is that the numerators of equation (19) vanish at the sonic radius. Therefore (Mathews & Bregman 1978),

$$r_s=\frac{3}{10\theta_s}\left[GM(r)+\frac{\dot{m}\Lambda(\theta_s)}{10\pi\theta_s M^2}\right]. \quad (20)$$

We have used two different dark matter profiles for the cluster. The first model (model A) has been discussed earlier in the literature in the context of cooling flows in clusters (White & Sarazin 1987; Wise & Sarazin 1993) with a density profile

$$\rho_d=\begin{cases}\dfrac{\rho_0}{1+(r/r_{\mathrm{core}})^2}+\dfrac{\rho_{0,g}}{1+(r/r_{c,g})^2} & \text{if } r<237\ \mathrm{kpc},\\ \dfrac{\rho_0}{1+(r/r_{\mathrm{core}})^2} & \text{if } r>237\ \mathrm{kpc}.\end{cases} \quad (21)$$

Here $\rho_0 = 1.8\times10^{-25}$ g cm^{-3} and $r_{\mathrm{core}} = 250$ kpc describe the profile of the cluster mass, and $\rho_{0,g} = 4.1\times10^{-22}$ g cm^{-3} and $r_{c,g} = 1.69$ kpc describe the profile of the galaxy in the center of the cluster.

Model B does not have the galaxy in the center, and so it is described simply by $\rho = \rho_0/[1+(r/r_{\mathrm{core}})^2]$.

With these assumptions, the solutions for steady cooling flows, $\dot{m} = \mathrm{const}$, are fully characterized by (1) the inflow rate, $\dot{m}$, and (2) the temperature of the gas, T_s, at the sonic radius r_s. Obviously, the cooling-flow solutions are only valid within the cooling radius r_{cool}, where $t_{\mathrm{cool}} = t_{\mathrm{age}}$. We assume a value of $t_{\mathrm{age}} = 10$ Gyr for all models. We assume that outside the cooling radius, gas obeys quasi-hydrostatic equilibrium (Sarazin 1986). Although this means matching the cooling-flow solutions with nonzero u to $u = 0$ solutions outside, in reality the velocity of gas at the cooling radius is very small (for $\dot{m} = 100\ M_\odot\ \mathrm{yr}^{-1}$ with $\rho \sim 10^{-26}$ g cm^{-3}, $r = 250$ kpc implies a velocity of 30 km s^{-1}), which is close to the limit of turbulence in the cluster gas (Jaffe 1980) and smaller than the sound velocity ($\sim 1.5\times10^3 (T/10^8\ \mathrm{K})^{1/2}$ km s^{-1}). The velocity of the flow at the cooling radius is therefore, for all practical purposes, sufficiently small to be matched to the solution of hydrostatic equilibrium outside. (In this approach, we avoid the time-consuming search for the critical value of $\dot{m}$ for which the flow solutions behave isothermally at $r \to \infty$; see Sulkanen, Burns, & Norman 1993.)

As in the usual assumptions for the interpretation of the SZ effect, we assume that the gas outside the cooling radius is isothermal, with a constant temperature profile. The density therefore obeys $\rho \propto [1+(r/r_{\mathrm{core}})^2]^{-3\beta/2}$, where $\beta = \mu m_p \sigma^2/k_B T_{\mathrm{iso}}$, and T_{iso} is the temperature of the gas at and outside the cooling radius.

For models with nonzero q (model C has the same mass profiles as model A), the solutions are characterized by T_s and the value of $\dot{m}$ at the cooling radius, $\dot{m}_{\mathrm{cool}}$. Since a fraction of mass drops out of the flow in this case, the inflow velocity need not rise rapidly, and so it is possible to find completely subsonic solutions.

3.2. *Cooling-Flow Solutions*

We numerically solved the flow equations for the parameters listed in Table 1. The density, temperature, and pressure profiles for three cases are presented in Figures 1, 2, and 3. We mark the position of r_{cool} in each case, and we mark r_s for the cases of transonic flows (when $\dot{m} = \mathrm{const}$). Beyond r_{cool}, we match a hydrostatic solution, as explained above, for the respective potentials. We also present, for

TABLE 1

PARAMETERS FOR COOLING-FLOW SOLUTIONS

Solution	Mass Model	q	$\dot{m}(r_{cool})$ ($M_\odot$ yr^{-1})	T_s (K)	r_s (kpc)	r_{cool} (kpc)	T_{iso} (K)
A1	A	0	100	6.5×10^6	0.688	127.5	1.2×10^8
A2	A	0	200	6.5×10^6	0.462	96.1	7.7×10^8
A3	A	0	300	6.5×10^6	0.712	132.2	7.7×10^8
B1	B	0	100	4.0×10^6	0.688	85.7	1.14×10^9
B2	B	0	200	6.5×10^6	0.462	89.6	1.9×10^9
B3	B	0	300	6.5×10^6	0.712	110.3	1.9×10^9
C1	A	3	200	...	...	111.6	1.1×10^8
C2	A	3	300	...	...	132.2	1.1×10^8

comparison, the behavior if the solutions outside r_{cool} are assumed to extend inward (that is, if no cooling flow is assumed). We postpone the discussion of the effect of these profiles on the SZ decrement to a later section, and only discuss the qualitative aspects of the solutions here.

The solution A1 is similar to that presented by Wise & Sarazin (1993; their Fig. 1, although they chose to characterize the solutions by the temperature at r_{cool} and not T_s, as we have done here). It is also similar (qualitatively) to the solution for A262 presented by Sulkanen et al. (1989). As the latter authors have noted, the effect of having a galactic potential in the center is to have a flatter temperature profile for $r > r_s$ than in the case of no galactic potential. This aspect is clearly seen while comparing our solutions with and without galactic potentials in the center. Our calculations for the case without the central galaxy are admittedly flawed in the very inner regions, where the gas density is larger than the dark matter density, which results in an incorrect determination of the gravitational potential in the inner region. However, this happens only inside a region ~ 25 kpc from the center, and should not influence our final results by a large extent.

A word of explanation regarding the pressure profiles is in order here. Naively speaking, it would appear that the

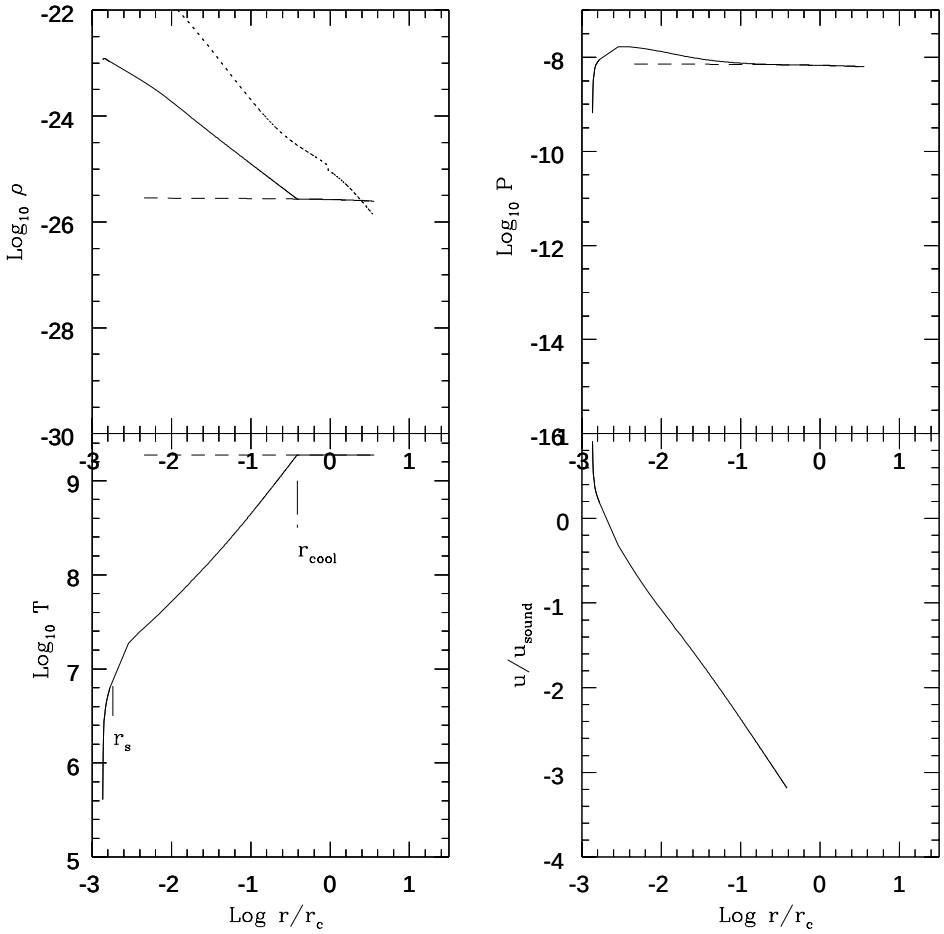

FIG. 1.—Cooling-flow solution A2. Top left panel shows the dark matter density profile (*dotted line*), the gas density profile for the cooling flow (*solid line*), and the corresponding case of gas in hydrostatic equilibrium. The bottom left panel shows the temperature profiles for the same cases. The position of r_s and r_{cool} are shown. The top right panel shows the pressure profiles, and the bottom right panel plots the Mach number of the cooling-flow gas as a function of the radius.

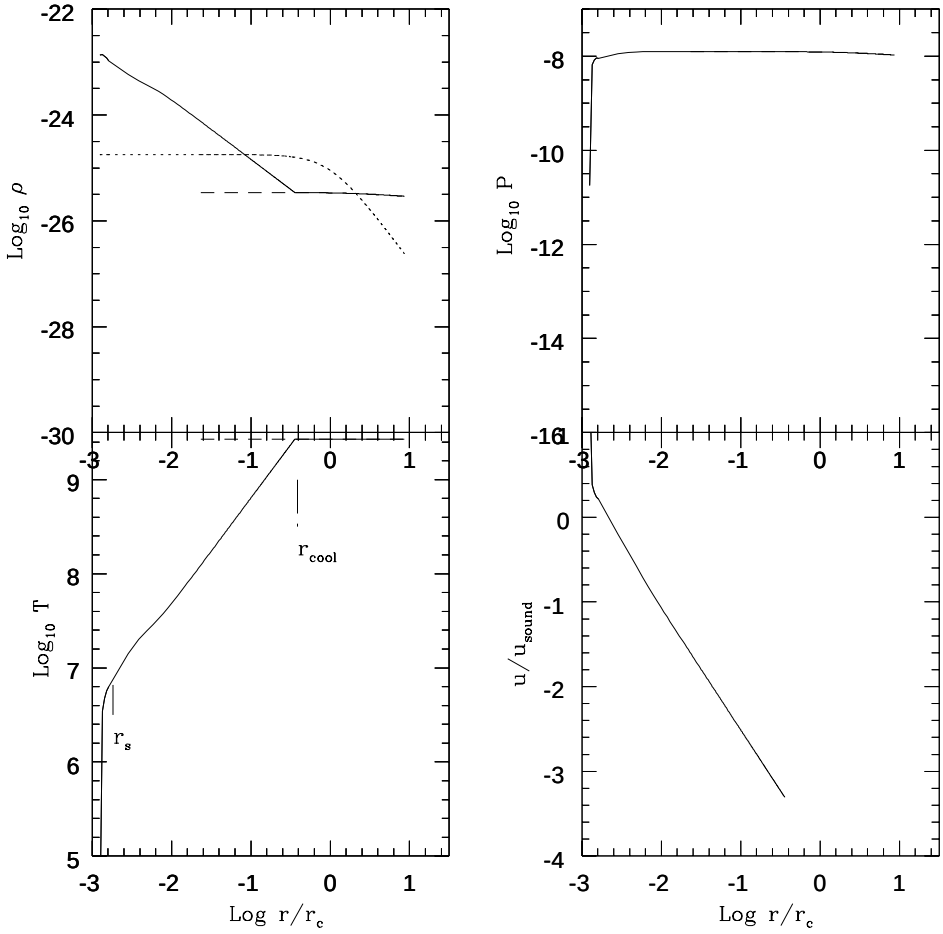

FIG. 2.—Same as Fig. 1, but for cooling-flow solution B2

pressure profile inside the cooling radius should have lower values than the corresponding case of hydrostatic equilibrium. The fact that it is not always so has been noted in the literature (e.g., Soker & Sarazin 1988; Fig. 1 of Sulkanen et al. 1989). The reason for the pressure bump just outside the sonic radius is that the flow in this inner region is driven not by pressure, but rather by gravity (see also Soker & Sarazin 1988). This is why the bump in the profile depends on the presence or absence of the galaxy in the center. This profile then leads to the curious result that the presence of a cooling flow can lead to the overestimation of the Hubble constant, as discussed in the next section.

A model with mass deposition (C1) is shown in Figure 3. The local mass flux is found to be almost proportional to the radius, consistent with various observations (Fabian et al. 1984; Thomas, Fabian, & Nulsen 1987), and therefore this is probably a realistic model for cooling-flow clusters. In this case, the temperature drops gradually all the way through, since the velocity does not rise too rapidly. The deposited mass is assumed to impart negligible pressure, and the pressure refers only to the gas taking part in the flow.

4. DETERMINATION OF THE HUBBLE CONSTANT

In this section we discuss the SZ and X-ray profiles of clusters with cooling flows. We compare these with profiles from clusters having gas in hydrostatic equilibrium, and comment on the reliability of measuring the Hubble constant. The effect of cooling flows and the subsequent increased Bremsstrahlung emission is seen in the sudden increase in the X-ray flux in the innermost region of the cluster (Fig. 4). The signature of the cooling flow is seen in the form of the central spike in the X-ray profile. The X-ray profile is only affected slightly by the drop in temperature, and it is the dependence on the gas density that holds. The temperature dependence becomes important only near the sonic point. Outside $r_{\rm cool}$, the X-ray profile is the same as that in the hydrostatic cases.

The SZ distortion is proportional to the line-of-sight integral of the pressure, and the sudden increase of the gas density inside the cooling radius is moderated by the decrease of the gas temperature. As a result, there is a gradual increase in the gas pressure. Near the sonic point, the temperature drops drastically by orders of magnitude, which results in a sudden decrease in pressure. However, since this change in pressure becomes acute only within $\approx 5\%$ of the core radius, it contributes negligibly to the line-of-sight integral of the gas pressure, and leads to an increase in the SZ distortion inside the cooling radius for all models considered (see Fig. 5). Like the X-ray profiles, the SZ profile outside $r_{\rm cool}$ is the same as that for the corresponding hydrostatic cases.

The SZ profiles have been calculated in the Rayleigh-Jeans limit ($x \ll 1$) where $j_\nu(x)$ of equation (4) goes to -2. In general, however, the profiles should be calculated using equation (2). Our results below are independent of the

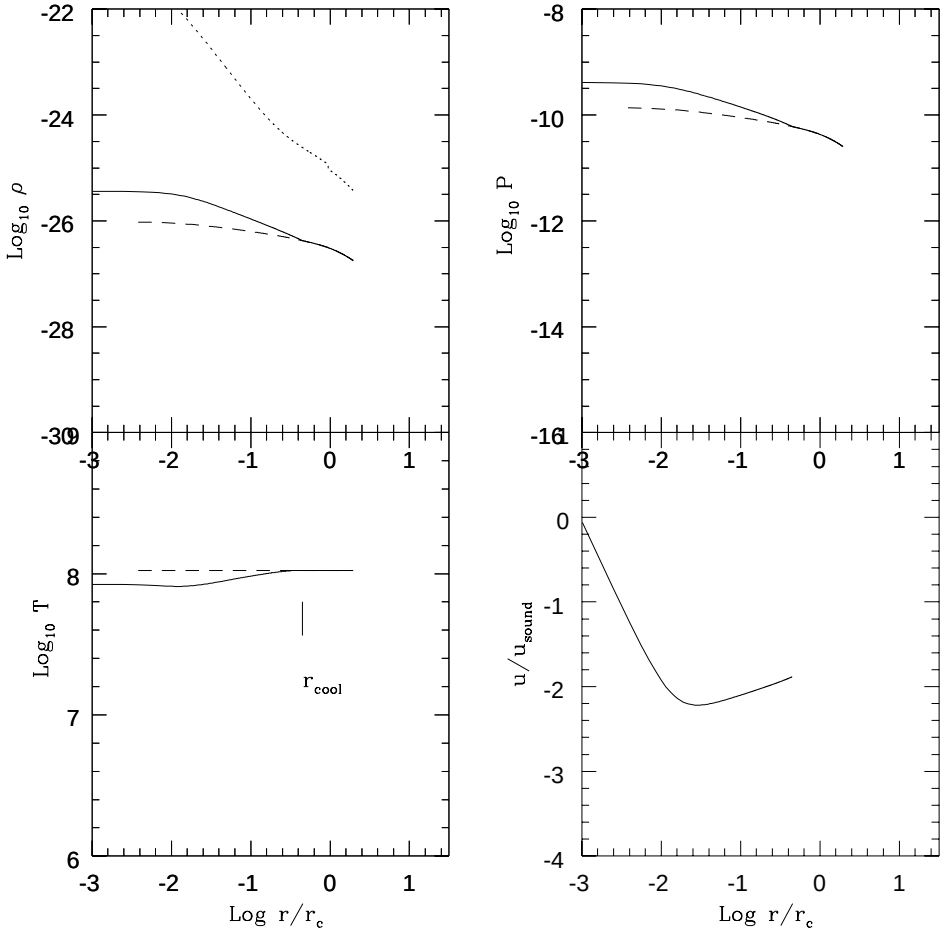

FIG. 3.—Same as Fig. 1, but for cooling-flow solution C1

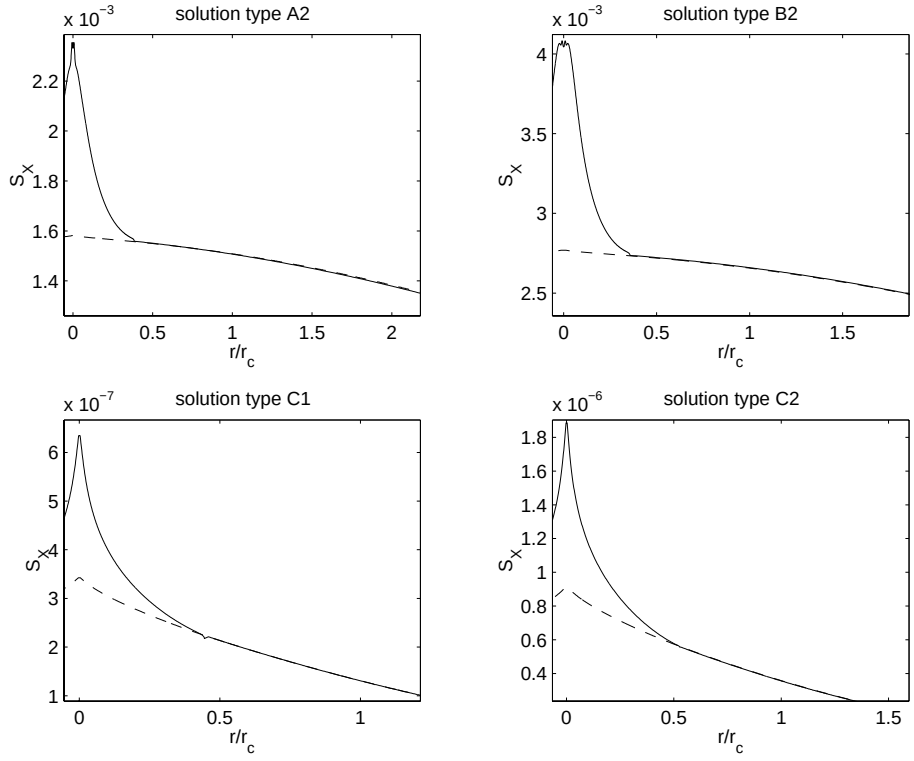

FIG. 4.—Unconvolved X-ray profiles for the solution types A2 (*top left*), B2 (*top right*), C1 (*bottom left*), and C2 (*bottom right*), for cooling-flow (*solid line*) and the corresponding cases of gas in hydrostatic equilibrium (*dashed line*). X-ray surface brightness in units of ergs s^{-1} cm^{-2} sr^{-1} is plotted against r/r_{core}. Individual plots have been magnified to highlight the differences between cooling-flow and hydrostatic cases.

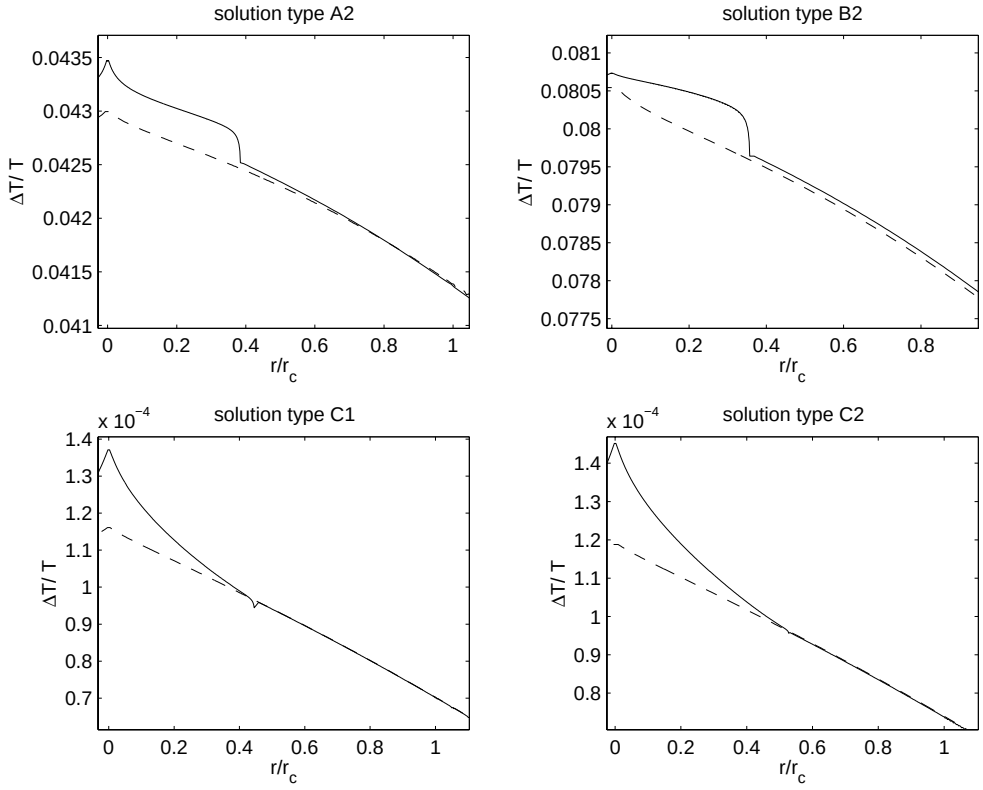

FIG. 5.—Unconvolved SZ profiles, for the solution types A2 (*top left*), B2 (*top right*), C1 (*bottom left*), and C2 (*bottom right*), for cooling-flow (*solid line*) and the corresponding cases of gas in hydrostatic equilibrium (*dashed line*). Here $\Delta T_{RJ}/T_{CMB}$ is plotted against r/r_{core}. Individual plots have been magnified to highlight the differences between cooling-flow and hydrostatic cases.

observational frequency, since the profiles at different frequencies have similar shapes, with the amplitude of the SZ distortion scaled either up or down.

Once both profiles are known, one can determine the deviation in the value of the Hubble constant using equations (14) and (16). The deviation from the idealized case can be parameterized as

$$f_H \equiv \frac{r_{\rm core,true}}{r_{\rm core,est,fit}} = \frac{H_{0,\rm est}}{H_{0,\rm true}} . \qquad (22)$$

The above formula has been used to determine the deviation of the estimated value of H_0 from the actual value, for models listed in Table 1. The effects of cooling flows on the determination of the cosmological parameters are summarized in Table 2.

To begin with, one must get best-fit values for $r_{\rm core}$ (or θ_c) and β from different profiles. Since the estimation of the Hubble constant depends on the determination of these parameters from the profiles, we look at this issue in more detail. We must keep in mind that the best-fit value of $r_{\rm core}$ (or θ_c) and β depend on whether one decides to fit the X-ray or the SZ profiles, and the choice can lead to significant differences in the estimated value of H_0. One of the reasons for the strong dependence on the nature of the profile could be the nonisothermality of the cluster gas. Recent observations indicate that intracluster gas has a temperature structure (see Markevitch et al. 1998). This is because the y-parameter depends on the integral over T_e, while the emissivity of thermal Bremsstrahlung depends on $T_e^{1/2}$. The dependence of the Gaunt factor on T_e is indirect and weak. Yoshikawa et al. (1998) have shown that a gas temperature drop in the central regions (their Fig. 3) should increase both $r_{\rm core}$ and β fitted to $y(\theta)$, and to a lesser extent to $S_X(\theta)$, as compared to those fitted to $n_e(r)$. This discrepancy increases at higher redshifts. However, in their case, there is little change in the gas density profile. Clumpiness can also give rise to different fits, resulting in an overestimation of the Hubble constant (Inagaki et al. 1995).

There are two other important points that should be kept in mind while fitting the profiles. First, we must remember that we are trying to fit a cluster having a finite profile with the formulae (eqs. [12] and [13]) for isothermal β profiles, which are derived assuming the cluster to be of infinite extent. This by itself can lead to an overestimation of H_0 (Inagaki et al. 1995). Thus, to have a good fit one must choose a segment of the profile such that, within that segment, the profiles (SZ or X-ray) for a finite cluster do not differ much from those of a *hypothetical* cluster of infinite extent. We found that SZ and X-ray profiles of clusters start

TABLE 2

EFFECT ON CENTRAL DECREMENT AND H_0 FOR $r_{\rm min} = 0.1 r_{\rm core}$

Solution Type	$H_{\rm est}/H_{\rm true}$	Δy_0 (% change)
A1	1.91	35
A2	1.18	11.5
A3	2.6	25
B1	1.36	12.0
B2	1.19	9.0
B3	1.13	8.5
C1	2.6	14.0
C2	2.7	11.3

TABLE 3

FITTING OF SZ PROFILE AND DEVIATION OF H_0 FOR $\dot{m} = 200\ M_\odot\ \mathrm{yr}^{-1}$

	$H/H_{\rm true}$		
SOLUTION TYPE	$r_{\rm min} = 0.2r_{\rm cool}$	$r_{\rm min} = 0.5r_{\rm cool}$	$r_{\rm min} = 0.8r_{\rm cool}$
A2	1.57	1.74	2.18
B2	1.44	1.58	2.06
C1	2.20	1.18	1.07

differing from those of infinite size at radii greater than 1.5 times the core radius. Hence, we have restricted our fitting to radii within $1.5r_{\rm core}$.

Next, one must also be careful to exclude the region close to the sonic point, so that the X-ray spike is excluded from the fit. In addition, the central portion in the SZ profile should be avoided, since its inclusion can give an *apparent* central decrement less than its neighboring points (see Schlickeiser 1991). We have fitted the SZ and X-ray profiles, varying the inner cutoff radius, and the results for a representative solution for each class of model are tabulated in Tables 3 and 4. Thus, all fittings were done for profiles extending from $r = r_{\rm min}$ to $r = 1.5r_{\rm core}$.

As can be seen from Table 2, cooling flows can lead to an overestimation of the Hubble constant. However, we must emphasize that it may not be possible to a priori estimate the amount of bias introduced in the measurement of the Hubble constant due to cooling flows. There is no simple correlation between the amount of cooling (i.e., $\dot{m}$) and the change in the estimated H_0 from the actual value. The total change depends not only on $\dot{m}$, but also on the position of the cooling radius, the sonic radius, the temperature at the sonic point, and the isothermal temperature characterizing the hydrostatic cases, with which comparisons are made. Specifically, the fitted values of $r_{\rm core}(\theta_c)$ and β for cooling-flow models differ from hydrostatic models according to the shape of the underlying profiles, which is marked by two important features: first, the central excess of X-ray flux (or excess decrement of SZ flux), and second, the deviation from the smooth hydrostatic profile inside $r_{\rm cool}$; the amount of overestimation mainly depends on these factors. For models with a central galaxy potential, there is always an overestimation of H_0, which is greater than in the models without the central galaxy.

For the realistic cases of models C1 and C2, where we have a variable $\dot{m}$ with r inside the cooling radius, the deviation of the estimated Hubble constant from its actual value is almost the same. It is also greater than that of models A and B, having similar mass flow rates. This may be due to the fact that the maximum deviation in pressure from the hydrostatic cases is more in nonsteady cases than in steady flows. In addition, nonsteady cases are marked by the absence of the sonic radii and the subsequent drop in temperature.

We note that although the different choice of fitting may change the absolute determination of cosmological parameters, the trend (i.e., deviation from the correct values) remains more or less unaffected. It is interesting to note that for the B-type model (C1), which includes mass deposition in cooling flows, the deviations decrease as one excludes a greater part of the cooling-flow region (Tables 3 and 4). The other models instead show an increase. Here we remind ourselves that models with mass deposition (i.e., B-type models) are more realistic (Fabian 1994). It is possible that the unusually high value of the deviation (Table 3) and the counterintuitive trend of increasing deviation with decreasing portion of cooling flow region used for fitting (Tables 3 and 4) arise because of the unrealistic modeling of cooling flows. If we take the model C1 as realistic, then Tables 3 and 4 show that to obtain a value of the Hubble constant within an accuracy of $\sim 10\%$, one should have $r_{\rm min} \sim 0.8r_{\rm cool}$. In most cases, $r_{\rm cool} < r_{\rm core}$ (Fabian et al. 1984). However, since $r_{\rm cool}$ cannot be determined without actually detecting a cooling flow in a cluster, we suggest that *a significant portion of the profile within $r_{\rm core}$ should be excluded as a precaution.* The SZ and the X-ray profiles for the different models are shown in Figures 4 and 5.

5. DISCUSSIONS AND CONCLUSION

Our work on the effect of the temperature structure of clusters and its effect on the SZ decrement differs from other previous works of this nature in following way: this work takes into account the change in density profile as well as the temperature profile, since both become important in the central region of the cluster. In addition, previous authors have looked at the issue of nonisothermality of a cluster at radii greater than the core radius of the cluster, whereas we look at temperature change in regions inside the core radius. For them, the density profile can still be well approximated by a β profile, whereas for cooling-flow solutions the density profile is vastly different. Furthermore, they have neglected radiative cooling in their work. We for the first time look at the SZ effect in the presence of radiative cooling, by first solving the cooling-flow equations for reasonable and physical solutions.

In summary, we find that the presence of a cooling flow in a cluster can lead to an overestimation of the Hubble constant determined from the Sunyaev-Zeldovich decrement. We have used different models of cooling flows, with and without mass deposition, and found the deviation in the estimated value of the Hubble constant in the case of a cooling flow from that of hydrostatic equilibrium. We have used the usual procedure of fitting the SZ and X-ray profile

TABLE 4

FITTING OF X-RAY PROFILE AND DEVIATION OF H_0 FOR $\dot{m} = 200\ M_\odot\ \mathrm{yr}^{-1}$

	$H/H_{\rm true}$			
SOLUTION TYPE	$r_{\rm min} = 0.5r_{\rm cool}$	$r_{\rm min} = 0.8r_{\rm cool}$	$r_{\rm min} = 0.9r_{\rm cool}$	$r_{\rm min} = 0.95r_{\rm cool}$
A2	...	4.7	2.7	1.7
B2	...	4.9	2.24	1.6
C1	1.69	1.12	1.02	≈ 1.0

with a β profile to get an estimated value of $r_{\rm core}$, and then compared this with the case of gas in hydrostatic equilibrium in order to estimate the deviation in the Hubble constant. For the more realistic models with mass deposition (varying $\dot{m}$ with radius), we found that the deviation decreases with the exclusion of greater portions of the cooling-flow region. Quantitatively, we found that for the deviation to be less than $\sim 10\%$, one should exclude a portion of the profile up to $\sim 0.8 r_{\rm cool}$. Since $r_{\rm cool}$ is difficult to estimate without actually detecting a cooling flow, we have suggested that a significant portion of the profile inside $r_{\rm core}$ should be excluded, to be safe.

There can be another important implication of the effect of cooling flows. With the upcoming satellite missions (*MAP* and *Planck*), we have come to the point where there are efforts to constrain Ω_0 with surveys of blank SZ fields (Bartlett, Blanchard, & Barbosa 1998; Bartlett 2000), ultimately giving rise to SZ-selected catalogs of clusters (Aghanim et al. 1997). This method relies on estimating the number of SZ sources brighter than a given threshold flux (Barbosa et al. 1996a). The point to be noted is that since these surveys are essentially flux-limited in nature, the validity of the analysis in determining Ω_0 depends crucially on the *one-to-one* association of flux limits to corresponding mass limits of clusters. From our analysis above, it seems that it may not be possible to associate a unique cluster mass with a given SZ distortion, given the uncertainty due to the presence of cooling flows. This might lead to contamination in SZ cluster catalogs and the inference of Ω_0. Recently, attempts have been made to constrain Ω_0 from variance measurement of brightness temperature in blank fields (Subrahmanyan et al. 1998), and comparing them to simulated fields (Majumdar & Subrahmanyan 2000) of cumulative SZ distortions from a cosmological distribution of clusters. These results may also be systematically affected by the presence of clusters having cooling flows.

The estimations made in this paper strictly apply to cases in which the image of the SZ effect is directly obtained by single-dish observations. For interferometric observations, the interferometer samples the Fourier transform of the sky brightness rather than the direct image of the sky. The Fourier conjugate variables to the right ascension and declination form the u-v plane in the Fourier domain. Due to spatial filtering by an interferometer, it is necessary that models be fitted directly to the data in the u-v plane, rather than to the image after deconvolution. We do not foresee drastic changes from our inferences in such cases, since the result mainly depends on the deviation of the SZ and X-ray profiles in the case of a cooling flow from those in the case of hydrostatic equilibrium. This, however, should be looked at in greater detail in future. We also note that with the growing number of high-quality images of the SZ effect with interferometers, which have greater resolution than single-dish antennas, the shape parameters of the clusters can be directly determined from the SZ data set rather than from an X-ray image (Grego et al. 2000).

Finally, we would like to add that although the calculations presented in this paper were done using the dark matter profile (eq. [21]) that is commonly used for calculating cooling flow solutions, it is inconsistent with the dark matter profile (Navarro et al. 1997) found in numerical simulations. (For a comparison of mass and gas distributions in clusters having cooling flows with different dark matter profiles, see Waxman & Miralda-Escudé 1995.) Moreover, we have neglected the self-gravity of the gas. Suto, Sasaki, & Makino (1998) have calculated the effect of including the self-gravity of the gas in determining the gas density profile. To make strong conclusions about the effect of cooling flows in the determination of the Hubble constant, one should take both the points mentioned above into account.

We are grateful to Joseph Silk for his comments on the manuscript. We also thank the referee, Asantha Cooray, for numerous suggestions which have helped us in improving the paper. One of the authors (S. M.) would like to thank the Raman Research Institute, Bangalore, for hospitality and for providing computational facilities. S. M. acknowledges help received from R. Sridharan in using IDL. Finally, he would also like to express his gratitude to Pijushpani Bhattacharjee for his constant encouragement.

REFERENCES

Aghanim, N., De Luca, A., Bouchet, F. R., Gispert, R., & Puget, J. L. 1997, A&A, 325, 9
Allen, S. W. 2000, MNRAS, 315, 269
Allen, S. W., Fabian, A. C., Johnstone, R. M., Arnaud, K. A., & Nulsen, P. E. J. 1999, MNRAS, submitted (preprint astro-ph/9910188)
Barbosa, D., Bartlett, J. G., Blanchard, A., & Oukbir, J. 1996a, preprint (astro-ph/9607036)
———. 1996b, A&A, 314, 13
Bartlett, J. G. 2000, A&A, submitted (preprint astro-ph/0001267)
Bartlett, J. G., Blanchard, A., & Barbosa, D. 1998, in Wide Field Surveys in Cosmology (Gif-sur-Yvette: Editions Frontières), 243
Bartlett, J. G., & Silk, J. 1994, ApJ, 423, 12
Birkinshaw, M. 1999, Phys Rep., 310, 97
Birkinshaw, M., & Hughes, J. P. 1994, ApJ, 420, 33
Blanchard, A., & Bartlett, J. G. 1998, A&A, 332, L49
Cavaliere, A., & Fusco-Femiano, R. 1978, A&A, 70, 677
Evrard, A. E. 1990, ApJ, 363, 349
Fabian, A. C. 1994, ARA&A, 32, 277
Fabian, A. C., Nulsen, P. E. J., & Canizares, C. R. 1984, Nature, 310, 733
Grego, L., Carlstrom, J. E., Joy, M. K., Reese, E. D., Holder, J. P., Patel, S., Cooray, A., & Holzapfel, W. L. 2000, ApJ, 539, 39
Herbig, T., Lawrence, C. R., Redhead, A. C. S., & Gulkis, S. 1995, ApJ, 449, L5
Holzapfel, W. L., et al. 1997, ApJ, 480, 449
Hughes, J. P., & Birkinshaw, M. 1998, ApJ, 501, 1
Inagaki, Y., Suginohara, T., & Suto, Y. 1995, PASJ, 47, 411
Jaffe, W. 1980, ApJ, 241, 925
Jones, M., et al. 1993, Nature, 365, 320
Kellog, E., Baldwin, J. R., & Koch, D. 1975, ApJ, 199, 299
Komatsu, E., Kitayama, T., Suto, Y., Hattori, M., Kawabe, R., Matsuo, H., Schindler, S., & Yoshikawa, K. 1999, ApJ, 516, L1
Majumdar, S., & Subrahmanyan, R. 2000, MNRAS, 312, 724
Makino, N., Sasaki, S., & Suto, Y. 1998, ApJ, 497, 555
Markevitch, M., Forman, W. R., Sarazin, C. L., & Vikhlinin, A. 1998, ApJ, 504, 27
Mathews, W. G., & Bregman, J. N. 1978, ApJ, 224, 308
Navarro, J. F., Frenk, C. S., & White, S. D. M. 1997, ApJ, 490, 493
Oukbir, J., & Blanchard, A. 1992, A&A, 262, L21
———. 1997, A&A, 317, 1
Peres, C. B., Fabian, A. C., Edge, A. C., Allen, A. W., Johnstone, R. M., & White, D. A. 1998, MNRAS, 298, 416
Pointecouteau, E., Giard, M., Benoit, A., Désert, F. X., Aghanim, N., Coron, N., Lamarre, J. A., & Delabrouille, J. 1999, ApJ, 519, L115
Reese, E. D., et al. 2000, ApJ, 533, 38
Rizza, E., Loken, C., Bliton, M., Roettiger, K., & Burns, J. 2000, AJ, 119, 21
Roettiger, K., Stone, J. M., & Mushotzky, R. F. 1997, ApJ, 482, 588
Sarazin, C. L. 1986, Rev. Mod. Phys., 58, 1
Sarazin, C. L., & Graney, C. M. 1991, ApJ, 375, 532
Sarazin, C. L., & White, R. E. 1987, ApJ, 320, 32
Saunders, R., et al. 1999, MNRAS, submitted (preprint astro-ph/9904168)
Schlickeiser, R. 1991, A&A, 248, L23
Schmutzler, T., & Tscharnuter, W. M. 1993, A&A, 273, 318
Silverberg, R. F., et al. 1997, ApJ, 485, 22
Soker, N., & Sarazin, C. L. 1988, ApJ, 327, 66
Subrahmanyan, R., Kesteven, M. J., Ekers, R. D., Sinclair, M., & Silk, J. 1998, MNRAS, 298, 1189

Sulkanen, M. E., Burns, J. O., & Norman, M. L. 1989, ApJ, 344, 604
Sunyaev, R. A., & Zeldovich, Ya. B. 1972, Commun. Astrophys. Space Phys., 4, 173
Suto, Y., Sasaki, S., & Makino, Y. 1998, ApJ, 509, 544
Thomas, P., Fabian, A. C., & Nulsen, P. E. J. 1987, MNRAS, 228, 973
Waxman, E., & Miralda-Escudé, J. 1995, ApJ, 451, 451
White, R. E., & Sarazin, C. L. 1987, ApJ, 318, 629
Wise, M. W., & Sarazin C. L. 1993, ApJ, 415, 58
Yoshikawa, K., Itoh, M., & Suto, Y. 1998, PASJ, 50, 203